# Combinatorial prospects of nanoparticle mediated immunotherapy of cancer

Silva, C.G. da

# 3

# THE EFFECT OF INJECTION ROUTE OF PLGA NANOPARTICLES ON THE BIODISTRIBUTION AND ICG BLOOD CLEARANCE RATE IN TUMOR BEARING MICE



Da Silva, C.G., Ossendorp, F., Cruz L.J.

*Manuscript in preparation*

CHAPTER 3

# Abstract

Poly(lactic-co-glycolic acid; PLGA) nanoparticles are used for cargo delivery in cancer treatments. We studied the biodistribution in the vital organs and ICG blood clearance rate upon injection of PLGA nanoparticles via the intratumoral, intravenous, and subcutaneous route in tumor bearing mice. For this purpose, we developed surrogate pegylated PLGA nanoparticles loaded with the near-infrared dye indocyanine green (ICG) for nanoparticle detection in the vital organs and to determine the ICG blood clearance rate.

## INTRODUCTION

There are several routes commonly chosen for nanoparticles administration in murine disease models for the optimal therapeutic efficacy and the induction of least adverse effects [1]. It has been well established that the physicochemical properties, such as size, shape, and surface charge, are key determinants of nanoparticles biodistribution and clearance [2]. Analysis of the optimal administration route of nanoparticles in preclinical research is important since it is pivotal for clinical translation and human application. Although there are only limited studies published, the biodistribution, clearance, and tumor uptake of inorganic carbon dots and of gold nanoparticles injected via several different routes have been determined [3–5]. The biodistribution of organic pegylated PLGA nanoparticles has been determined for the intravenous and oral routes on healthy mice but relatively under-examined on mice bearing tumors [6–8]. Most cancer treatments require a high concentration of drugs in the tumor to

attain their therapeutic effect, and as low as possible elsewhere in the healthy tissue to limit adverse effects. Therefore, it is common to leverage the maximum attainable drug concentration possible in the tumor against the maximum acceptable instances and/or severity of the adverse effects, which limits the anti-cancer therapeutic effects. Cancer drugs are most administered via the intravenous (IV) or oral route which enables the (bio)distribution and accumulation of the drugs throughout all tissue, including the tumor. One strategy to improve the drug accumulation ratio in the tumor versus healthy tissue is the intratumoral (IT) administration of cancer drugs. When the drugs are loaded into PLGA nanoparticles and injected via the IT route, it is possible to attain high drug concentration and local slow release of the drugs in the tumor.
In this study, we set to determine the biodistribution of ICG-loaded nanoparticles in the vital organs and tumors when administered either via the IV, IT, or subcutaneous (SC) route in tumor bearing mice. In addition, we determined the ICG blood clearance rate upon the distinct administration routes.



## MATERIALS AND METHODS

**Materials and reagents**

The PLGA polymer (lactide/glycolide molar ratio of 48:52 to 52:48) was purchased from Boehringer Ingelheim (Ingelheim am Rhein, Germany). Dichloromethane (DCM; CAS 75-09-2 CH2CL2 MW 84.93) and polyvinyl alcohol (PVA; CAS 9002-89-5) were purchased from Sigma-Aldrich (Zwijndrecht, The Netherlands). Chloroform (CHCL3 MW 119.38 g/mol) was purchased from Merck (Darmstadt, Germany). Lipid-PEG 2000 (1,2-Distearoyl-sn-Glycero-3-Phosphoethanolamine-N-[Methoxy(Polyethylene glycol)-2000]; powder MW 2805.54) was purchased from Avanti Polar Lipids (AL, USA). ICG dye was purchased from Sigma-Aldrich.

**Synthesis of the ICG-loaded pegylated PLGA NPs**

The NPs were synthesized in an oil/water emulsion, using a solvent evaporation-extraction method as per described elsewhere [9,10]. Briefly, a 1.5 mL solution of DCM was prepared that contained 50 mg of PLGA and 0.5 mg of ICG dye. Next, the solution was added dropwise to 10 mL of aqueous 2.5% (w/v) PVA and emulsified for 120 s using a sonicator (250 watts; Sonifier 250; Branson, Danbury, USA). A new beaker was prepared that contained an air-dried solution of 10 mg of Lipid-PEG 2000 dissolved in 0.1 mL of chloroform. The previous solution containing the ICG dye was transferred to the new beaker that contained the Lipid-PEG film and the whole solution was

homogenized for 60 s by sonication and stored overnight at 4 °C under continuous stirring to allow evaporation of the solvent. Using ultracentrifugation (12,800 rpm for 30 minutes) and washing with distillated water (4x) at 4 °C the NPs were collected. Finally, the NPs were ready after 3 days of lyophilization.

**Physicochemical properties of the NPs**

The average size, polydispersity index and surface charge (zeta-potential) of the NPs were determined by dynamic light scattering. A sample of 50 µg of the NPs was dissolved in 1 mL of ultrapure MilliQ H2O and measured for size using a Zetasizer (Nano ZS, Malvern Ltd., UK). By using the same device and sample, the NPs surface charge was determined by the laser Doppler electrophoresis method.

**Cell lines**

The murine tumor cell line TC-1 (a gift from T.C. Wu, Johns Hopkins University, Baltimore, MD, USA) was generated by retroviral transduction of lung fibroblasts of C57BL/6 origin, to express the HPV16 E6 and E7 genes and the activated human c-Ha-ras oncogene [11]. The TC-1 cell line was cultured in DMEM medium (BioWhittaker, Verviers, Belgium) supplemented with 8% heat-inactivated fetal calf serum (FCS; Greiner bio-one, Alphen a/d Rijn, The Netherlands), penicillin (50 µg/mL; Gibco, Paisley, Scotland), streptomycin (50 µg/mL; Gibco), L-glutamine (2 mM; Gibco), β-mercaptoethanol (20 µM; Sigma, Saint Louis, USA), and Geneticin (G418; 400 µg/mL). Furthermore, regular PCR analysis was performed to assure the cells were free of mycoplasma and common rodent viruses.

**Mice strains**

C57BL/6 (H-2b haplotype) and Balb/c female mice, between 8 to 12 weeks of age, were purchased from Charles River ('s-Hertogenbosch, The Netherlands). The mice were housed at the animal facility of Leiden University Medical Center under specific pathogen free conditions. All animal experiments were approved by the Dutch Central Committee on Animal Experimentation and were strictly conducted according to the Dutch animal welfare law.

**Biodistribution and blood analysis**

The relative signal quantification in vital organs was performed by SC syngeneic inoculation with $1x10^5$ TC-1 cells in 0.2 mL PBS in the right flank of C57BL/6 mice. When the tumors became established, at nine days after tumor inoculation, 50 µL containing

500 µg of NPs (10 mg/mL) dissolved in PBS were administered either IT, SC (left flank) or IV via caudal vein injection. Approximately 25 µL of blood was collected from the caudal vein after 5, 120, 240, and 360 minutes, and 24 hours after the injection of NPs. Upon collection of the last blood sample the mice were euthanized, and the spleen, heart, kidneys, liver, lungs and tumors removed for further ex vivo analysis. The ICG-signal emitted from the organs and the blood was detected using a Li-Cor Odyssey scanner (Li-Cor Biosciences, Lincoln, NEBR, USA) set to scan at 800 nm and analysis were conducted using the Li-Cor Odyssey v3.0.21 software.



The overview images were acquired by following the same treatment protocol as described above. However, these experiments were performed on Balb/c mice inoculated SC with $3x10^5$ CT-26 cells in 0.2 mL PBS in the right flank and the images were acquired using the IVIS Spectrum In Vivo Imaging System (PerkinElmer, Ohio, USA) and the Living Image Software version 4.7 (PerkinElmer).

## RESULTS

**Physicochemical properties and in vitro characterization of the NPs**

For this study, we synthesized PLGA NPs loaded with ICG near-infrared dye in an oil/water emulsion using a solvent evaporation-extraction method and the surface functionalized with pegylation. The ICG-loaded NPs were characterized for size and surface charge (Table 1). The size of the ICG-loaded NPs was found to be 268 nm on average (Table 1, Fig. 1A) and the surface charge –21 mV (Table 1, Fig. 1B). The ICG signal in the ICG-loaded NPs was positively detected with an IVIS Spectrum in vivo imaging system (Figure 1C).

**Table 1. Physicochemical characterization of PLGA NPs**

| NP | Size ± SD (nm) | PDI | ζ Potentia ± SD (mV)l |
|---|---|---|---|
| NP(ICG) | 267.6 ± 81.0 | 0.412 | -21.7 ± 7.7 |

Physicochemical characterization of ICG-loaded NPs. The NPs were characterized by dynamic light scattering and zeta potential measurements. The size and zeta potential data represent the mean value ± SD of 10 readings.

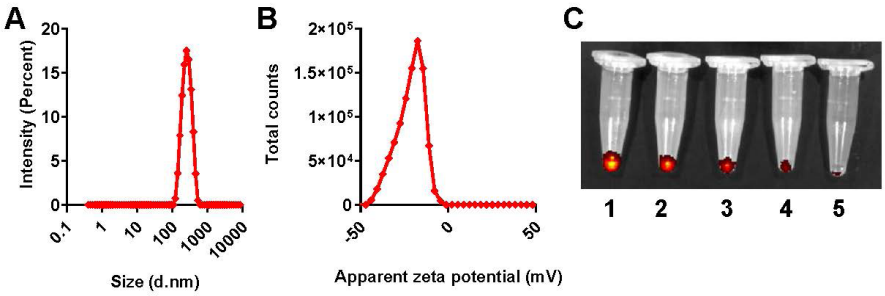


**Figure 1. The NP size and zeta potential data characterized by dynamic light scattering. The size (A)** and zeta potential **(B)** data distributions represent the mean value ± SD of 10 readings. **(C)** A picture showing positive detection of the ICG-loaded NPs in a dilution series of the NPs in PBS acquired by the IVIS Spectrum in vivo imaging system set to acquire at excitation 745 nm and emission 800 nm. The annotated numbers correspond to the nanoparticle concentration used, as follows: 1) 5 mg/mL; 2) 2.5 mg/mL; 3) 1.25 mg/mL; 4) 0.63 mg/mL; 5) 0.31 mg/mL in a total volume of 50 µLin each Eppendorf tube.

### Tumor accumulation after IV, SC or IT administration of ICG-loaded NPs

To determine whether the concentration of ICG in the tumor would differ after IV, SC or IT administration of ICG-loaded NPs, tumor-bearing mice were euthanized after 24 hours post injection and analyzed by IVIS fluorescence imaging. The sites of SC and IT injection of the ICG-loaded NPs were detectable (Figure 2A). The tumor with the highest ICG signal was the tumor treated via an IT injection (Figure 2B). However, no ICG signal in the tumor could be detected after SC or IV injection by IVIS fluorescence imaging in the CT-26 cancer model.

**Figure 2. Anatomical and multiple organ overview of the ICG-loaded NPs biodistribution in mice bearing subcutaneous CT-26 tumors upon IV, IT, and SC injection routes. A)** Representative anatomical photographs of mice with a subcutaneous tumor of mice administered with ICG-loaded NPs (50 µL at 10 mg/mL) via IV, IT or SC injection routes acquired with the IVIS Spectrum in vivo imaging system after 24 hours. Photographs above are bright fields and photographs from below are an overlay with the ICG fluorescence signal. **B)** Representative photographs of relevant mice organs administered with ICG-loaded NPs via IV, IT or SC injection routes acquired with the IVIS Spectrum in vivo imaging system. Photograph from the left side is the bright field and the photograph from the right side is an overlay with the ICG fluorescence signal. 1: tumor; 2: spleen; 3: liver; 4: kidneys; 5: lungs; 6: heart.

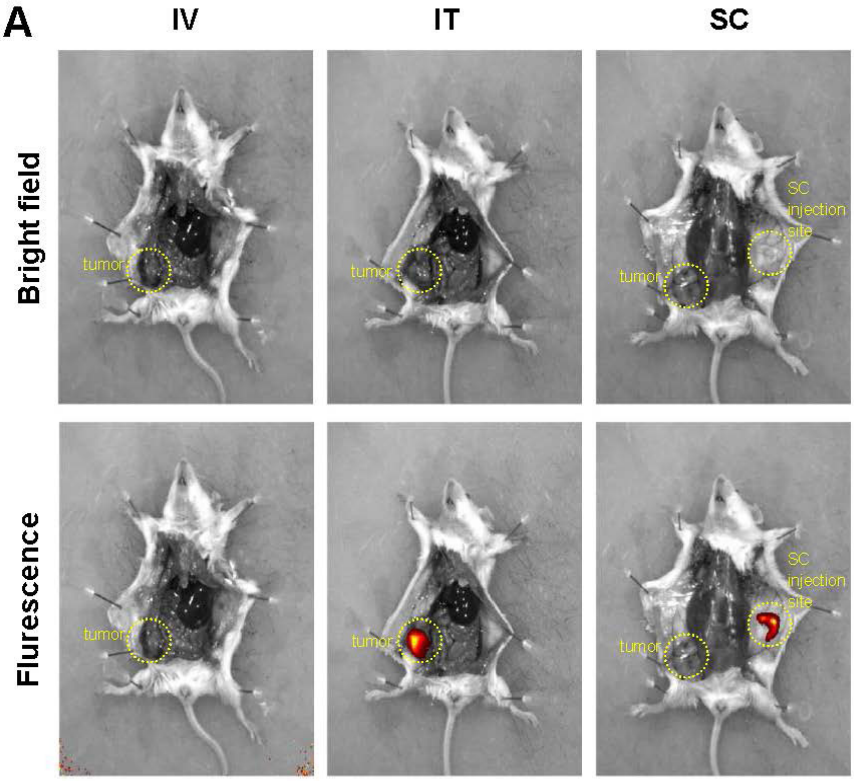
A
IV
IT
SC
Bright field
Flurescence
tumor
SC injection site

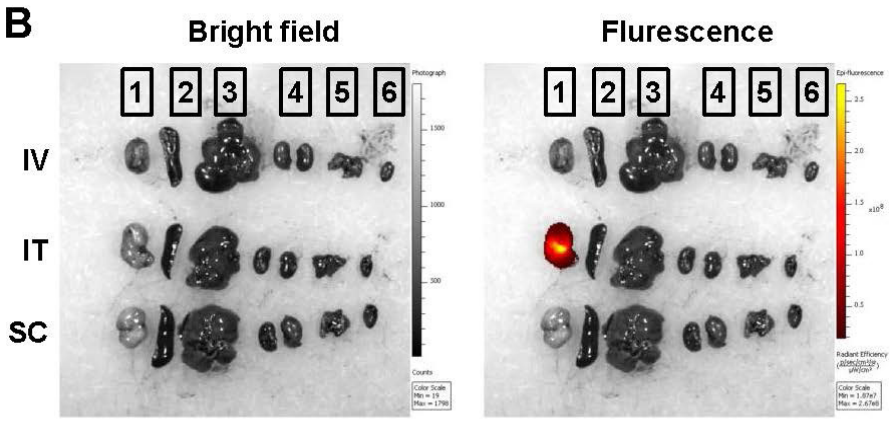
B
Bright field
Flurescence
IV
IT
SC
1
2
3
4
5
6

**Distinct organ accumulation and blood concentration upon distinct injection routes of ICG-loaded NPs**

To determine the ICG blood clearance rate after IV, SC or IT administration of ICG-loaded NPs, blood was collected at several intervals post-injection. The Li-Cor Odyssey scanner was used to acquire the relative quantitative signal instead of the IVIS Spectrum in vivo imaging system as it was found to be more sensitive (lower detection limit) to the ICG signal in the organs and blood. The IV route yielded the highest concentration of ICG measured 5 minutes after injection, while the SC route was observed to be slightly higher than the IT route (Figure 3A). After 120 minutes post-injection, the ICG blood concentration rapidly decreased for the IV and IT route and then remained stable for up to 24 hours. However, after 120 minutes the ICG blood concentration of the SC route was found to increase and to gradually decrease after 240 and 360 minutes; after 24 hours the SC route depicted similar concentrations of that of IV and IT routes (Figure 3A). After 24 hours, the organs of the mice were removed and the ICG concentration measured (Figure 3B). The ICG concentration of the IT route was found to be slightly elevated in the spleen, kidneys and liver, but not in the heart or lungs, and up to 800-fold higher in the tumor compared to the IV or SC route. The ICG concentration of the IV route was higher in the liver compared to SC route but not in the other organs.

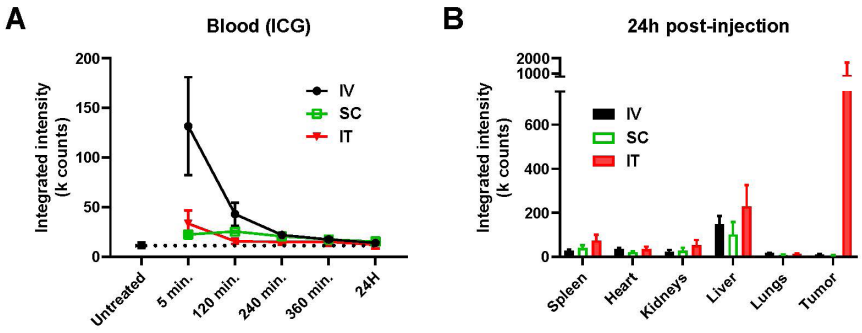


**Figure 3. Relative quantification of ICG in mice organs bearing subcutaneous TC-1 tumors and ICG blood concentration in time upon IV, SC or IT injection routes of ICG-loaded NPs.** **A)** ICG blood concentration measured after 5, 120, 240, and 360 minutes, or 24 hours after injection. **B)** Biodistribution of ICG-loaded NPs measured in the spleen, heart, kidneys, liver, lungs, and TC-1 tumors in mice 24 hours after injection. The relative signal quantification from the blood and vital organs was acquired by using the Li-Cor Odyssey scanner. The organ signal data was made specific by subtracting the background fluorescence from each corresponding organ from untreated mice.

## Discussion

Here we have shown that the IV, SC, or IT injection routes of pegylated PLGA nanoparticles loaded with ICG display a distinct biodistribution and blood clearance rate. There is low accumulation of the nanoparticles in the vital organs and the accumulation is higher in the liver then in the kidneys, which suggest that these types of nanoparticles are likely cleared via the hepatic route. The nanoparticle tumor accumulation was considerably higher when the nanoparticles were injected IT and very low when injected IV and SC, respectively. When the nanoparticles design is to deliver their cargo to the tumor area, and the tumor is accessible, the IT injection route would be the preferred administration route to achieve highest accumulation possible in the tumor area. Interestingly, the nanoparticle accumulation was also higher in the spleen for the IT route, which could indicate that (immune) cells from the tumor area take-up the nanoparticles (or their cargo) and migrate to the spleen. This observation also adds to the evidence reported by us and others that the IT administration of nanoparticles loaded with immune modulators or other immune stimulating cancer drugs can induce immune abscopal effects relevant for the control of metastases [9,10,12]. Nonetheless, the downside of IT administration is that the nanoparticles are

unlikely to reach metastases themselves and if the abscopal effect is absent or weak, the IV or SC route would be preferred. Alternatively, it would also be possible to treat accessible tumors IT and IV to reach the metastases. However, by combining the IT and IV administration, the rate of adverse effects is likely to increase. Moreover, the clinical practice of the administration of cancer drugs directly in the tumor of cancer patients, even in less accessible tumors such as liver cancers, is increasing due to improved methods and procedures [13]. The additional advantage of nanoparticles when injected IT, is their slow and sustained release capability, which makes them often better alternatives to non-nanoparticle drugs to exert prolonged pharmacological effects in the tumor area. The data in this report clearly shows considerably higher concentration of ICG in the tumor after 24 hours post IT injection compared to IV or SC administration, and in a previous report we have shown that nanoparticles can remain in the tumor area even after 168 hours [9]. Additionally, many cancer drugs are deleteriously toxic to vital organs such as the heart, lungs, and kidneys, which already lead to the development of Doxil®, the FDA approved pegylated nanoparticle loaded with doxorubicin [14]. The pegylated PLGA nanoparticles presented in this report also displayed favorable low biodistribution in these vital organs. Despite the pegylated layer, the nanoparticles are rapidly removed from the blood reaching very low levels after 360 minutes and below detection limit after 24 hours regardless of the injection route. This observation is in line with reports that blood circulation half-life increases from 30 minutes (without PEG coating) to 5 hours (with PEG coating) but seldomly longer for similar nanoparticles [15–17]. Although also the IV administration route, and to a lower extent the SC route, induced low but detectable signal emanating from the tumor, the signal likely came from nanoparticles that accumulated via the 'enhanced permeability and retention' effect [18]. However, the accumulation appears low and since the blood circulation time is relatively short, the IV injection route does not appear to be an efficient route to achieve a high accumulation in the tumor in the tested cancer models.

Although the fluorescence detection method used in this study is increasingly used in biodistribution studies, the results should be taken into consideration carefully. Namely, the ICG-detection method used here is qualitative and semi-quantitative and can only aid as an indicator of relative ICG-signal concentration. Several factors, including signal quenching, dequenching, and saturation, as well as limited tissue depth penetration, can influence the acquired signal [19]. Nonetheless, quantification by fluorescence from tissue homogenates versus planar (2D) fluorescence reflectance imaging of excised intact organs, as used in this study, was shown representative to

whole organ lysates [20]. And, besides the advantage of non-exposure to ionizing radiation, optical imaging has proven a reliable method for qualitative measurement of NPs biodistribution [21].

# REFERENCES


[1] D. Chenthamara, S. Subramaniam, S.G. Ramakrishnan, S. Krishnaswamy, M.M. Essa, F.H. Lin, M.W. Qoronfleh, Therapeutic efficacy of nanoparticles and routes of administration, Biomater. Res. 23 (2019). https://doi.org/10.1186/s40824-019-0166-x.

[2] H.S. Choi, W. Liu, F. Liu, K. Nasr, P. Misra, M.G. Bawendi, J. V. Frangioni, Design considerations for tumour-targeted nanoparticles, Nat. Nanotechnol. 5 (2010) 42–47. https://doi.org/10.1038/nnano.2009.314.

[3] X. Huang, F. Zhang, L. Zhu, K.Y. Choi, N. Guo, J. Guo, K. Tackett, P. Anilkumar, G. Liu, Q. Quan, H.S. Choi, G. Niu, Y.P. Sun, S. Lee, X. Chen, Effect of injection routes on the biodistribution, clearance, and tumor uptake of carbon dots, ACS Nano. 7 (2013) 5684–5693. https://doi.org/10.1021/nn401911k.

[4] X.D. Zhang, H.Y. Wu, D. Wu, Y.Y. Wang, J.H. Chang, Z. Bin Zhai, A.M. Meng, P.X. Liu, L.A. Zhang, F.Y. Fan, Toxicologic effects of gold nanoparticles in vivo by different administration routes, Int. J. Nanomedicine. 5 (2010) 771–781. https://doi.org/10.2147/IJN.S8428.

[5] M. Bednarski, M. Dudek, J. Knutelska, L. Nowiński, J. Sapa, M. Zygmunt, G. Nowak, M. Luty-Błocho, M. Wojnicki, K. Fitzner, M. Tęsiorowski, The influence of the route of administration of gold nanoparticles on their tissue distribution and basic biochemical parameters: In vivo studies, Pharmacol. Reports. 67 (2015) 405–409. https://doi.org/10.1016/j.pharep.2014.10.019.

[6] B. Semete, L. Booysen, Y. Lemmer, L. Kalombo, L. Katata, J. Verschoor, H.S. Swai, In vivo evaluation of the biodistribution and safety of PLGA nanoparticles as drug delivery systems., Nanomedicine. 6 (2010) 662–71. https://doi.org/10.1016/j.nano.2010.02.002.

[7] Y.P. Li, Y.Y. Pei, X.Y. Zhang, Z.H. Gu, Z.H. Zhou, W.F. Yuan, J.J. Zhou, J.H. Zhu, X.J. Gao, PEGylated PLGA nanoparticles as protein carriers: Synthesis, preparation and biodistribution in rats, J. Control. Release. 71 (2001) 203–211. https://doi.org/10.1016/S0168-3659(01)00218-8.

[8] K.S. Yadav, K. Chuttani, A.K. Mishra, K.K. Sawant, Effect of size on the biodistribution and blood clearance of etoposide-loaded PLGA nanoparticles, PDA J. Pharm. Sci. Technol. 65 (2011) 131–139.

[9] C.G. Da Silva, M.G.M. Camps, T.M.W.Y. Li, L. Zerrillo, C.W. Löwik, F. Ossendorp, L.J. Cruz, Effective chemoimmunotherapy by co-delivery of doxorubicin and immune adjuvants in biodegradable nanoparticles., Theranostics. 9 (2019) 6485–6500. https://doi.org/10.7150/thno.34429.

[10] C.G. Da Silva, M.G.M. Camps, T.M.W.Y. Li, A.B. Chan, F. Ossendorp, L.J. Cruz, Co-delivery of immunomodulators in biodegradable nanoparticles improves therapeutic efficacy of cancer vaccines, Biomaterials. 220 (2019) 119417. https://doi.org/10.1016/j.biomaterials.2019.119417.

[11] K.Y. Lin, F.G. Guarnieri, K.F. Staveley-O'Carroll, H.I. Levitsky, J.T. August, D.M. Pardoll, T.C. Wu, Treatment of established tumors with a novel vaccine that enhances major histocompatibility class II presentation of tumor antigen., Cancer Res. 56 (1996) 21–6.

[12] X.Y. Chu, W. Huang, Y.L. Wang, L.W. Meng, L.Q. Chen, M.J. Jin, L. Chen, C.H. Gao, C. Ge, Z.G. Gao, C.S. Gao, Improving antitumor outcomes for palliative intratumoral injection therapy through lecithin– chitosan nanoparticles loading paclitaxel– cholesterol complex, Int. J. Nanomedicine. 14 (2019) 689–705. https://doi.org/10.2147/IJN.S188667.

[13] W.X. Hong, S. Haebe, A.S. Lee, C.B. Westphalen, J.A. Norton, W. Jiang, R. Levy, Intratumoral Immunotherapy for Early-stage Solid Tumors, Clin. Cancer Res. 26 (2020) 3091–3099. https://doi.org/10.1158/1078-0432.CCR-19-3642.

[14] S. Tran, P.-J. DeGiovanni, B. Piel, P. Rai, Cancer nanomedicine: a review of recent success in drug delivery., Clin. Transl. Med. 6 (2017) 44. https://doi.org/10.1186/s40169-017-0175-0.

[15] R. Gref, Y. Minamitake, M.T. Peracchia, V. Trubetskoy, V. Torchilin, R. Langer, Biodegradable long-circulating polymeric nanospheres, Science (80-. ). 263 (1994) 1600–1603. https://doi.org/10.1126/science.8128245.

[16] A.L. Klibanov, K. Maruyama, V.P. Torchilin, L. Huang, Amphipathic polyethyleneglycols effectively prolong the circulation time of liposomes, FEBS Lett. 268 (1990) 235–237. https://doi.org/10.1016/0014-5793(90)81016-H.

[17] J.S. Suk, Q. Xu, N. Kim, J. Hanes, L.M. Ensign, PEGylation as a strategy for improving nanoparticle-based drug and gene delivery, Adv. Drug Deliv. Rev. 99 (2016) 28–51. https://doi.org/10.1016/j.addr.2015.09.012.

[18] J.W. Nichols, Y.H. Bae, EPR: Evidence and fallacy, J. Control. Release. 190 (2014) 451–464. https://doi.org/10.1016/j.jconrel.2014.03.057.

[19] F. Meng, J. Wang, Q. Ping, Y. Yeo, Quantitative Assessment of Nanoparticle Biodistribution by Fluorescence Imaging, Revisited, ACS Nano. 12 (2018) 6458–6468. https://doi.org/10.1021/acsnano.8b02881.

[20] K.O. Vasquez, C. Casavant, J.D. Peterson, Quantitative Whole Body Biodistribution of Fluorescent-Labeled Agents by Non-Invasive Tomographic Imaging, PLoS One. 6 (2011) e20594. https://doi.org/10.1371/journal.pone.0020594.

[21] L. Arms, D.W. Smith, J. Flynn, W. Palmer, A. Martin, A. Woldu, S. Hua, Advantages and limitations of current techniques for analyzing the biodistribution of nanoparticles, Front. Pharmacol. 9 (2018) 802. https://doi.org/10.3389/fphar.2018.00802.